Laser-Tissue Interactions

2

Rudolf Steiner

Core Messages

› Understanding laser-tissue interactions and using the laser in an optimal way are the most important messages in this chapter.

› The wavelength-dependent penetration depth of laser light into tissue determines heat flow and the thickness of the zone of necrosis.

› The concept of photothermolysis, introduced by Rox Anderson, improved specificity of laser-tissue interactions.

› Thermal lasers are used for tissue coagulation and vaporisation.

› For tissue ablation, high absorption of the laser light by the tissue is necessary, as is high power density of the laser pulse (>100 kW/cm²).

› Keep in mind that the shorter the laser pulse or the laser irradiation on the same spot, the smaller will be the zone of necrosis.

› Consider possible acoustic side effects with short and ultrashort laser pulses.

2.1 Optical Properties of Tissue

To understand the various modalities of laser-tissue interaction, it is necessary to get an overview of how photons penetrate biological tissue and how physics dominates their behaviour. When photons strike the surface of the tissue, because of the refractive index change, a portion (4–10%) of the photons are reflected according to the angle of incidence. Photons penetrating the surface initially are refracted, obeying the law of Snellius, which states that photons entering a medium with a higher refractive index are refracted towards the vertical axis to the surface (Fig. 2.1). The refractive index of tissue (n_{tissue}) is ~1.4. Snellius' law states:

$$\frac{\sin \alpha_1}{\sin \alpha_2} = \frac{n_2}{n_1} = n_{12}.$$

In the tissue, the photons may be scattered, changing their direction of flight according to the probability function expressed as the anisotropy factor, g, or absorbed, exciting the absorbing molecule by an electronic transition.

2.1.1 Absorption

The energy states of molecules are quantized; therefore, absorption of a photon takes place only when its energy, $E = h\nu$, corresponds to the energy difference between such quantized states.

Absorption of a photon by a chromophore causes either a quantized change in the distance between charges (electron transition, ultraviolet or visible spectrum; Fig. 2.2) or a quantized change of vibrational modes of the molecule (vibration transition, near infrared [NIR]; Fig. 2.3).
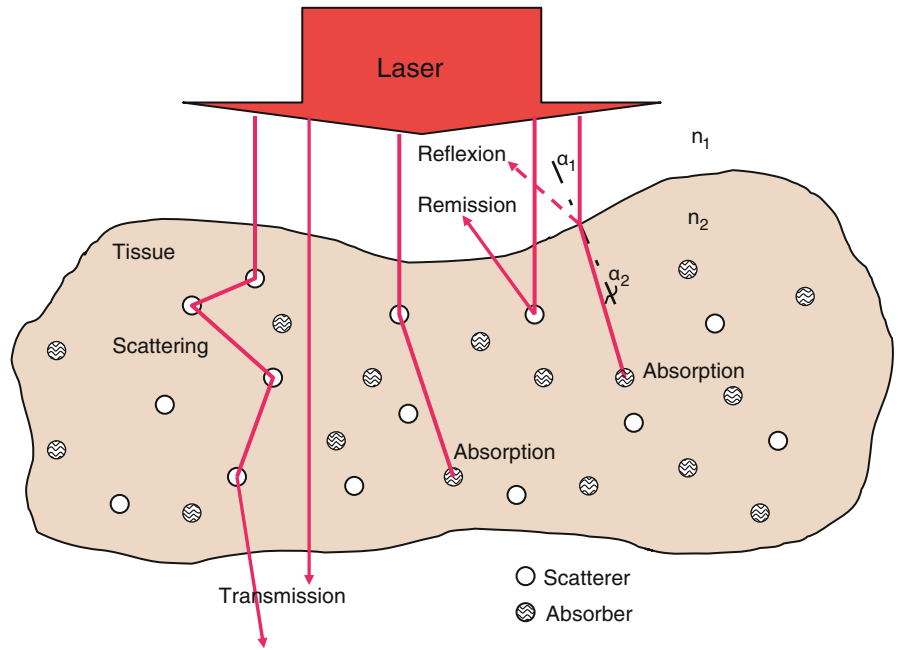
Absorbing molecular components of the tissue are porphyrin, haemoglobin, melanin, flavin, retinol, nuclear acids, deoxyribonucleic acid (DNA)/ribonucleic acid (RNA), and reduced nicotinamide adenine dinucleotide,

R. Steiner
Institut für Lasertechnologien in der Medizin und
Meßtechnik an der Universität Ulm, Helmholtzstraße 12,
89081, Ulm, Germany
e-mail: rudolf.steiner@ilm.uni-ulm.de

Fig. 2.1 Optical behaviour of a tissue layer during irradiation with laser light

Laser

Reflexion

Remission

n_1

α_1

n_2

Tissue

Scattering

Absorption

Absorption

Transmission

○ Scatterer

⊛ Absorber

Electronic transitions (UV and visible light)

E

S_1

4
3
2
1
$V'=0$

S_0

$V=0$

pyrroles
porphyrins
heme
(chlorophyll)
cytochromes
phycobiliproteins
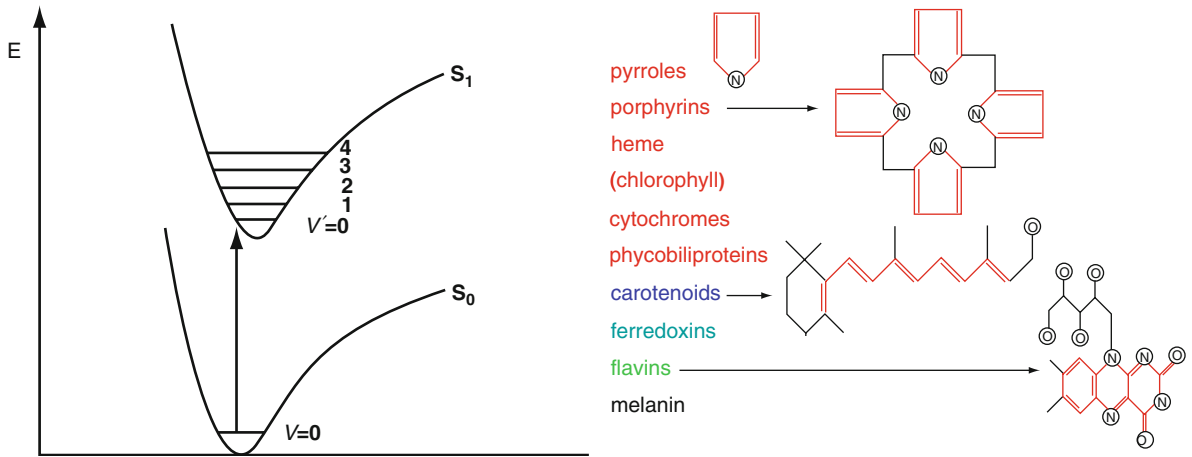carotenoids
ferredoxins
flavins
melanin

Fig. 2.2 Scheme of electronic excitation after photon absorption and a list of some chromophores in the tissue with the chemical structure. *UV* ultraviolet
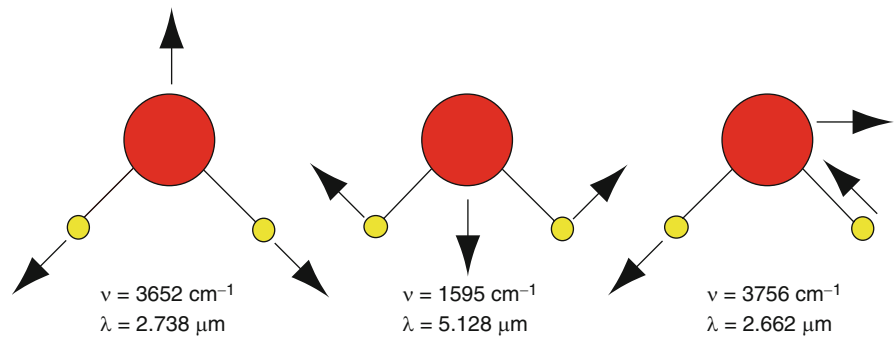
UV ultraviolet

Fig. 2.3 Vibration transitions of a water molecule with its absorption bands

$\nu = 3652$ cm^{-1}
$\lambda = 2.738$ μm

$\nu = 1595$ cm^{-1}
$\lambda = 5.128$ μm

$\nu = 3756$ cm^{-1}
$\lambda = 2.662$ μm

where electronic transitions are excited, leading to discrete and intense (broad) absorption bands. In the NIR and mid-infrared (MIR) region, tissue absorption is dominated by water absorption, with the maximum at 3 μm. The coefficient μ_a (cm^{-1}) characterizes the absorption. The inverse, l_a, defines the penetration depth (mean free path) into the absorbing medium.

To understand the mechanism of absorption, one can imagine a chromophore with a geometrical cross-section of size A (cm^2) being placed in a parallel laser beam (Fig. 2.4). The shadow it creates is the effective cross-section σ_a (cm^2), which in most cases is smaller than the
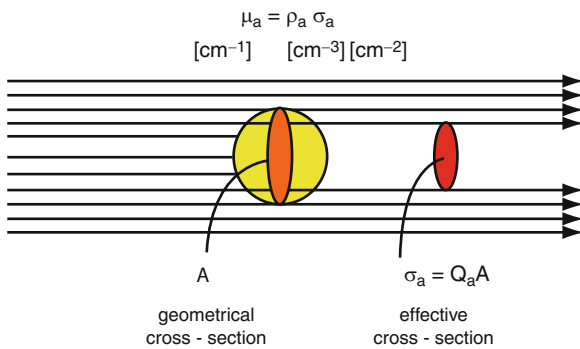

Fig. 2.4 Definition of the absorption coefficient by the cross-section of chromophores and their volume densities

geometrical cross-section A. When there are a lot of chromophores in a solution with volume density ρ_a (cm^{-3}), then the absorption coefficient is $\mu_a = \rho_a \sigma_a$ (cm^{-1}).

Chemists normally use Beer's law when they calculate the transmission of light through a cuvette of a dimension, d, filled with absorbing liquid. Then the expression for the transmission, T, is

$$T = I / I_0 = 10^{-\varepsilon c d} = 10^{-\rho}$$

where:

- ε: molar extinction coefficient [L/mol·cm]
- c: concentration of chromophores [mol/L]
- l: optical path (cm)
- ρ: optical density (OD) or extinction

Physicists, however, describe the transmission, T, as

$$T = I / I0 = \exp(-\sigma_a N_a l) = \exp(-\mu_a l),$$

where:

- σ_a: effective cross-section of absorption (cm^2)
- N_a: density of the absorbing molecules (cm^{-3})
- l: optical path (cm)
- μ_a: absorption coefficient (cm^{-1})

The absorption spectra of different chromophores of biological tissue and water are plotted in Fig. 2.5.
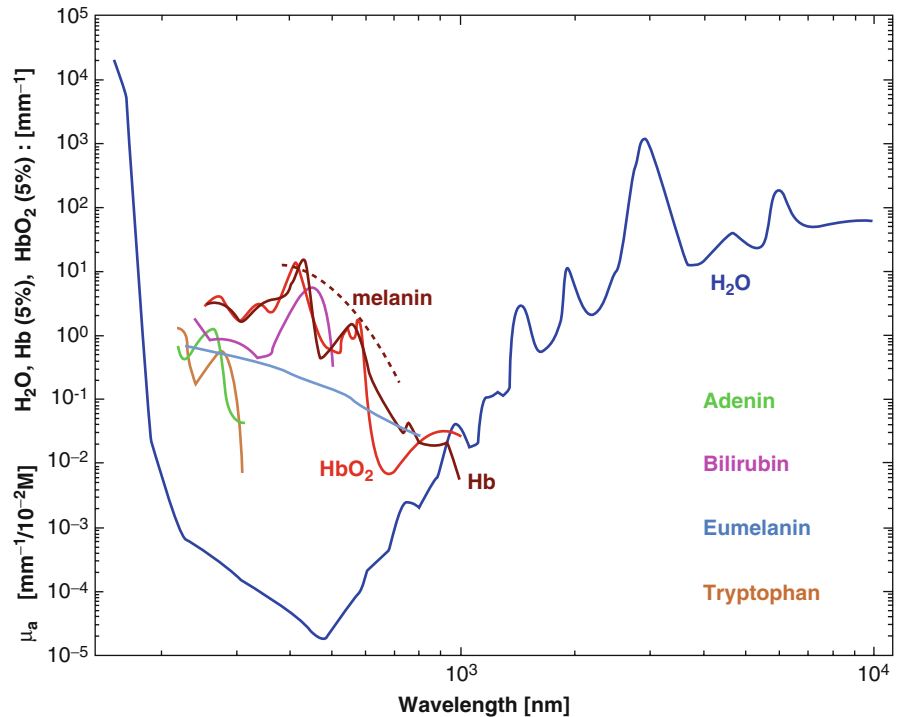

Fig. 2.5 Absorption spectra of chromophores in biological soft tissue

2.1.2 Scattering

The scattering behaviour of biological tissue is also important because it determines the volume distribution of light intensity in the tissue. This is the primary step for tissue interaction, which is followed by absorption and heat generation. Scattering of a photon is accompanied by a change in the propagation direction without loss of energy. Scattering structures of the tissue can be *macroscopic* like muscle fibres, skin layers, or dentin tubules; *microscopic* like cells or intracellular structures; and even *sub-microscopic*, taking into account macromolecules or nanoparticles.

According to the size of the scattering structure, one has to distinguish between Rayleigh scattering, $d << \lambda$, and Mie scattering, $d \geq \lambda$. Scattering of tissue is always a combination of Rayleigh and Mie scattering (see Fig. 2.6), depending on what structures are dominant. Rayleigh scattering is rather isotropic, only depending on the polarisation and the wavelength. The scattering cross-section is inverse to λ^4, which makes the sky "blue." The equation for Rayleigh scattering is:

$$Q_s = \frac{128\pi^4 a^4}{3\lambda^4} \left| \frac{n_s^2 - n^2}{n_s^2 + 2n^2} \right|.$$

Mie scattering, near-field as well as far-field, can be calculated exactly with a Monte Carlo simulation (MCS). Forward scattering is pronounced and is demonstrated in Fig. 2.7, which gives an example of the scattering behaviour of a water droplet of 10 μm in size at a wavelength of 650 nm. Because of the large size of the droplet, one gets interference of scattered light from different locations within the droplet. This results
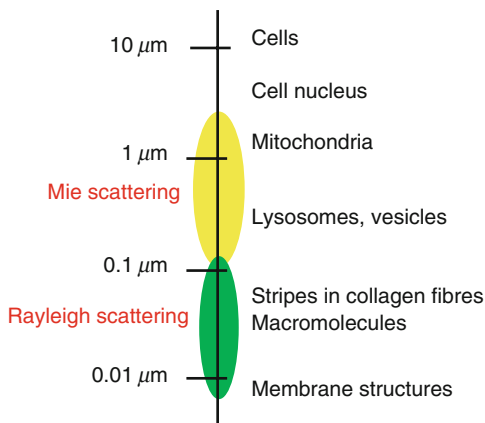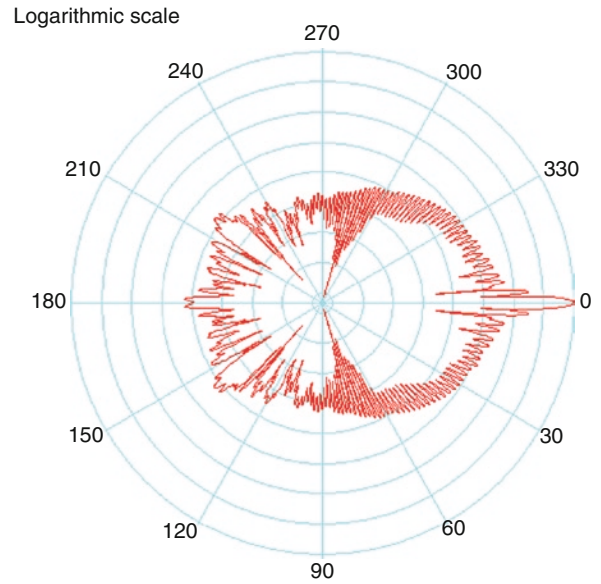
Fig. 2.7 Mie scattering of a water droplet that is 10 μm in size at $\lambda = 650$ nm

in intensity maxima when measuring the angle-resolved scattering.

The scattering, similar to absorption, is expressed by the scattering coefficient μ_s (cm^{-1}). The inverse parameter, $1/\mu_s$ (cm), is the mean free path length until a next scattering event occurs. As a rule of thumb, one can say that for red light in the human skin, the mean free path length for absorption is 50 μm, and the mean free path length for scattering is 5 mm. This means that, statistically, a photon is scattered 100 times until it is absorbed.

We have seen from Mie scattering that scattering is not isotropic. Forward scattering is predominant in biological tissue. This characteristic is described by the anisotropy factor g. g can have absolute values from 0 to 1, from isotropic scattering ($g = 0$) to forward scattering ($g = 1$). Negative values for g stand for backward scattering. In tissue, g can vary from 0.8 to 0.99.

Anisotropy factor g: $0 \leq g \leq 1$. $g = 0$: isotropic scattering; $g = 1$: forward scattering.

Taking into account the g value, a reduced scattering coefficient, μ_s' (cm^{-1}), is defined as

$$\mu_s' = \mu_s(1-g).$$

In MCSs, one has to consider a probability function for g in what direction a photon is scattered. The Henyey-Greenstein phase function [7] $p(\theta)$ is often used to describe the angular distribution of light scattered by tissue. It is characterized by the average cosine $<\cos \theta>$

Fig. 2.6 Rayleigh and Mie scattering of tissue structures

of the scattering angle, θ. Since the Henyey-Greenstein phase function is a probability density function, it is normalized to an area of 1 (Fig. 2.9). This model has been applied to numerous situations, ranging from the scattering of light by biological tissue to scattering by interstellar dust clouds. The angular distribution of scattered light is given by

$$p(\theta) = \frac{1}{4\pi} \frac{1-g^2}{(1+g^2-2g\cos(\theta))^{3/2}}.$$

The parameter g characterizes the normalized distribution. For some values of g, Fig. 2.8 shows the probability of scattering from $-180° \le \theta \le +180°$. When g approaches the value 1, then the function is very peaked around $\theta = 0$. In case of isotropic scattering, $g = 0$, there is a constant value of $1/4\pi$ over all scattering angles θ.

The sum of μ_s and μ_a is called the total attenuation coefficient μ_t (cm^{-1}):

$$\mu_t = \mu_s + \mu_a \ (\text{cm}^{-1}).$$

Measuring the optical constants of biological tissues is not a simple task. In a configuration where a collimated beam hits a tissue sample of defined thickness and only the transmitted photons (ballistic photons) reach the detector, the attenuation coefficient μ_t can be measured.

In general, the optical parameters of tissue like μ_a, μ_s, and g cannot be measured directly. Very complex measuring and evaluation processes are needed to determine such parameters. When a slice of tissue is placed between two integrating spheres (Ulbricht spheres), then the total transmitted and diffusely reemitted radiation can be measured. MCS helps to extract the values of the optical parameters by iteration procedures.
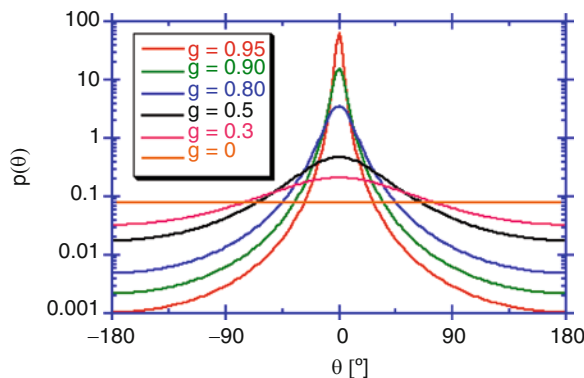
Some other expressions are helpful to describe the optical properties of biological tissue. The fraction of the scattering μ_s over the total attenuation μ_t is called Albedo a:

$$Albedo \ a = \mu_s/(\mu_s + \mu_a)$$

Whereas the effective damping coefficient μ_{eff} is defined as:

$$\mu_{eff} = (3\mu_a(\mu_a + \mu_s'))^{1/2} \ (\text{cm}^{-1}).$$

The inverse value $1/\mu_{eff}$, is called the effective penetration depth, d_{eff}, of light into tissue:

$$d_{eff} = 1/\mu_{eff} \ (\text{cm}),$$

and the effective mean free path length, X_{eff}, is as follows:

$$X_{eff} = 1/(\mu_a + \mu_s') \ [\text{cm}].$$

The equation

$$I(d) \ \alpha \ I_0 e^{-\sqrt{3\mu_a(\mu_a+\mu_s^e)}d} = I_0 e^{-\mu_{eff}d}$$

describes approximately the portion of the power of light or photon density, which is transported over a distance d. Photons may propagate undisturbed or may reach the detection surface element after multiple scatterings. If scattering is predominantly in a forward direction, then the transport (reduced) scattering coefficient μ_s' is considerably smaller than μ_s. Single photons arriving at the detector element may have passed a much longer path length (multiple scattering) than distance d.

Photon density penetration into tissue also can be described approximately by the diffusion

$$\frac{\partial}{\partial t}\rho(\vec{r},t) - Dc_m\Delta\rho(\vec{r},t) + \mu_a c_m\rho(\vec{r},t) = q_0(\vec{r},t).$$

With the diffusion constant D,

$$D = \frac{1}{3(\mu_a + \mu_s')}$$

No analytical solution exists, however, for the transport equation modelling the light penetration into biological tissue. Therefore, in most cases, the MCS [18] has to be used to determine the photon distribution in the tissue. Programmes are available on and can be downloaded free from the Internet. MCS is also useful to model laser-tissue interactions. One example was published by Romero et al. [12].

Fig. 2.8 Henyey-Greenstein probability function for different g values

Table 2.1 A summary of penetration depths in muscle tissue at different laser wavelengths

Wavelength (nm)	Penetration depth ($1/\mu_a$ [µm])	Effective optical penetration ($1/\mu_{eff}$ [µm])
193	≈ 10	≈ 1
308	50	6
532	830	240
1.064	2.500	1.900
2.060	286	250
2.940	3	3
10.600	17	17

The decision of the appropriate model to calculate the photon distribution and penetration into tissue depends on the values for μ_a and μ_s' [17]. Several cases can be distinguished:

$\mu_a \gg \mu_s'$: Lambert-Beers' law ($\lambda < 300$ nm and $\lambda > 2{,}000$ nm)

$\mu_a \ll \mu_s'$: the diffusion approximation is valid (650 nm $< \lambda < 1{,}150$ nm)

$\mu_a \approx \mu_s'$: the transport equation with MCS is valid (300 nm $< \lambda < 650$ nm; $1{,}150$ nm $< \lambda < 2{,}000$ nm).

Table 2.1 summarizes the penetration depth in muscle tissue at different laser wavelengths. The mean free path due to absorption and the effective penetration have been considered [3].

It is possible to measure the light distribution inside tissue by introducing a miniaturized probe of 100-µm diameter into the tissue via the hollow needle of a syringe. The measurements confirm the theoretically derived phenomenon that the light intensity directly below the tissue surface is enhanced by a factor of 2–4 as compared with the intensity of the incident beam [15]. The increased fluence rate is caused by scattered photons overlapping with the incident photons. Another observation is that, due to the scattering effect, the penetration depth depends on the irradiated area. Consequently, the penetration depth will double if, for the same irradiance, the beam diameter increases from 1 to 5 mm. For dermatological applications, this effect has to be taken into account. For deep light penetration when treating port wine stains or for hair removal, 10- to 15-mm spot diameters of the laser are recommended.

The measured intensity inside the tissue is called the *fluence rate*. It is the power absorbed by a small sphere divided by the cross-section of the sphere: $A = \pi R^2$.

Fluence rate: $F = P/A$ (W/cm²)

The depth of penetration of laser light into tissue is greatest in the wavelength range of 700–900 nm (optical window). Blood, water, and melanin are the main absorbing components in the tissue (Fig. 2.5). Therefore, Ar⁺ lasers, dye lasers, and diode lasers effectively interact with blood, the Alexandrite laser with melanin, and MIR lasers with the water content of the tissue.

2.2 Reaction Mechanisms

The first systematic presentation of the reaction mechanisms of lasers with tissue was by Boulnois [3] in 1986 (Fig. 2.9). Another important finding was the "selective photothermolysis" (SP) by Anderson and Parish in 1983 [1, 2]. SP is the damage confined to the specific tissue structures by selection of laser wavelength, regulation of pulse duration, and repetition rate.

In the following section we consider the different laser-tissue interaction mechanisms.

2.3 Non thermal, Chemical Reactions

In low-dose irradiation of living tissue, photons may have an influence on the proliferation of cells. Much literature has been published in the past about the interaction of photons (633-nm helium-neon laser or an 820-nm diode laser) with in vitro cell cultures [11] and wound healing by biostimulation. Most of the results, however, were not verified or generated under controlled condition.

2.3.1 Biostimulation

It is well accepted that the energy of photons when absorbed in cells or tissue may affect cellular metabolism and signalling pathways. A review is given by Hawkins-Evans and Abrahamse [6].

Molecular targets can be cytochrome c oxidase (with absorption in the NIR) or photoactive porphyrins. Cellular targets are mitochondria with the effects of increased adenosine triphosphate production, modulation of reactive oxygen species, and initiation of cellular signalling [5], as illustrated in Fig. 2.10.

Fig. 2.9 Plot of laser-tissue interaction mechanisms over time of interaction. Modified from Boulnois JL. Photophysical processes in recent medical laser developments: a review. Lasers Med Sci. 1986;1:47–66 [3]
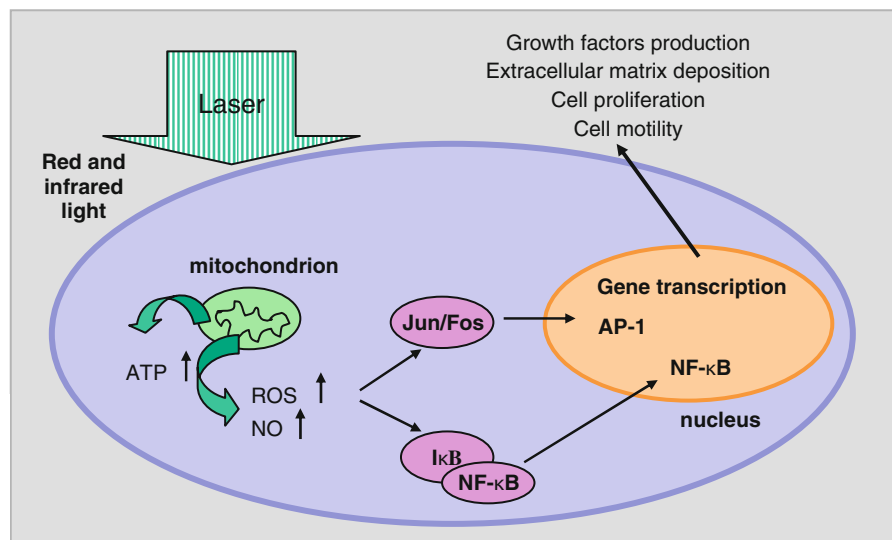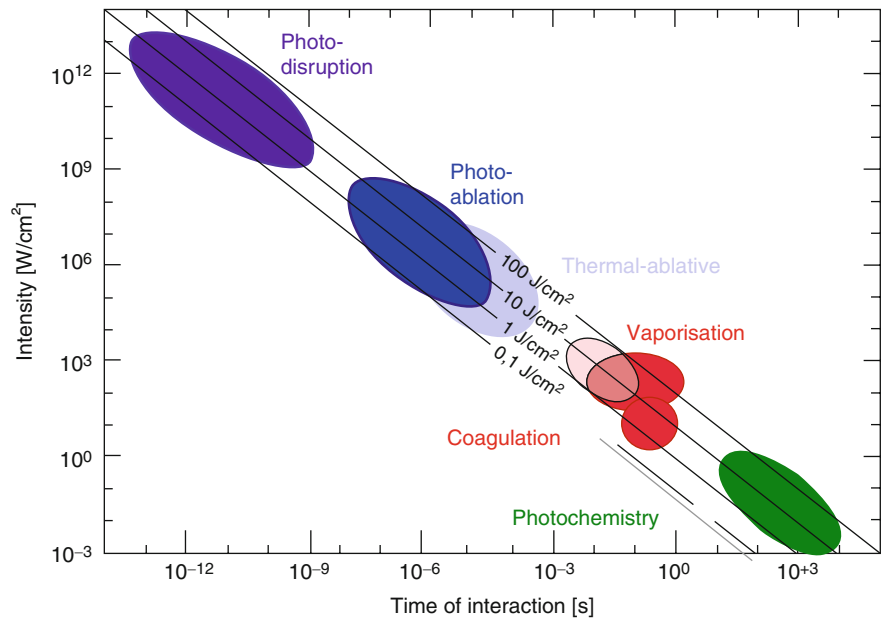

Fig. 2.10 Cell signalling pathways induced by low-level laser therapy. *ATP* adenosine triphosphate, *ROS* reactive oxygen species, *NO* nitric oxide

The results may be:

- Increased cell proliferation and migration (particularly by fibroblasts).
- Modulation in the levels of cytokines, growth factors, and inflammatory mediators.
- Influence on the activity of second messengers (cyclic adenosine monophosphate, Ca^{2+}, nitric oxide).
- Increased tissue oxygenation.
- Increased healing of chronic wounds and improvements in injuries and carpal tunnel syndrome, pain reduction, and impact on nerve injury.

In all cases, the light dose has to be selected carefully because more light is not always better. Spectral regions that show the highest effect of activation are around 633, 690, 820 and 900 nm.

2.3.2 Photodynamic Therapy

Photodynamic therapy (PDT) uses a photochemical reaction with three components: light for activation, sensitizers, and molecular oxygen. The sensitizer molecules
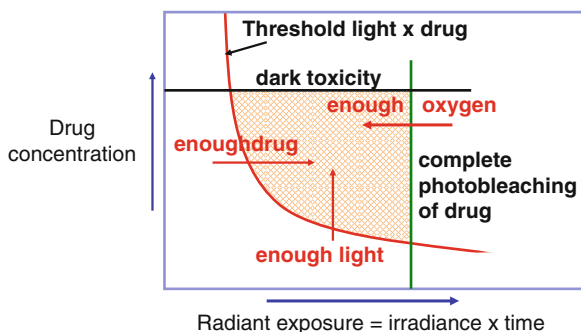
Fig. 2.11 Treatment window for photodynamic therapy

are accumulated in the target cellular structure. They absorb the photons and become excited. After energy transformation from a singlet state to a long-lived triplet state by intersystem crossing, the energy is transferred to oxygen. The excited oxygen (singlet oxygen or radical) destroys the cell. This phototoxic reaction is used in tumour treatment but also in the treatment of precancerous stages or nonmalignant lesions. Sensitizers are also fluorescent. Therefore, they are used for tumour diagnosis and imaging, for example, to visualize bladder tumours in early stages. PDT is described in detail in Chap. 28 of this book.

Here, it is illustrated in the graph of Fig. 2.11 that PDT has a treatment window depending on drug concentration, dark toxicity, radiant exposure of laser light, and sufficient oxygen supply. Therefore, dosimetry is very important for a successful treatment to control all these parameters, especially in deeper layers of the tissue. Sensitizer concentration accumulated in the target tissue and photobleaching during irradiation can be monitored by increase or decrease of the fluorescence intensity.

2.4 Thermal Reactions

The energy of laser irradiation is transferred into heat due to the absorption of the photons by tissue components, DNA/RNA, chromophores, proteins, enzymes, and water. According to the degree of heating, stepwise and selective thermal damage can be achieved:

42–45°C: beginning of hyperthermia, conformational changes, and shrinkage of collagen;
50°C: reduction of enzymatic activity;
60°C: denaturation of proteins, coagulation of the collagens, membrane permeabilisation;

100°C: tissue drying and formation of vacuoles;
>100°C: beginning of vaporization and tissue carbonisation;
300–1,000°C: thermoablation of tissue, photoablation and disruption.

The corresponding pathologic analysis of photothermal effects is well described by Thomsen [16]. Examples of coagulation and tissue vaporization are presented in Fig. 2.12.

The laser irradiation that is absorbed by the tissue will heat the tissue, and the temperature increase, ΔT, is given by the absorbed thermal energy per unit volume, Q (J/cm³), divided by the density, ρ (g/cm³), and the specific heat, c_w [J/g°K]:

$$\Delta T = Q/\rho c_w \ [°K]$$

Thermal diffusion is responsible for heat flow into the tissue. If the exposure time with a laser pulse, t_p, is short compared to the diffusion time, t_d, then we have *"thermal confinement"* and the pulse energy is converted into heat [10, 13, 14] in a tissue volume determined by the inverse absorption coefficient, $1/\mu_a$, and the spot size, d. The diffusion time is

$$t_d = 1/\kappa \mu_a^2 \ [s].$$

The thermal diffusion coefficient κ (m²/s) is determined by the thermal conductivity, Λ [W/m°K], divided by the density and specific heat:

$$\kappa = \Lambda/\rho c_w \ (m²/s).$$

Table 2.2 summarizes the thermal coefficients for different biological tissue materials.

Thermal diffusion and the extent of tissue necrosis are related. With low laser power and long irradiation time, thermal necrosis is large. Shortening the laser application time reduces the time for thermal diffusion, and the zone of necrosis becomes smaller. Minimum thermal necrosis is reached when the irradiation time is equal to the thermal diffusion time or thermal relaxation time. Nevertheless, it will not be smaller than the wavelength-dependent penetration depth of the laser light into the tissue.

Thermal damage of the tissue is described by the Arrhenius rate equation. The consequence of this equation is that the threshold for tissue damage depends on the laser power and the application time. This threshold can be reached with high laser power in a very short time, resulting in a higher temperature, or with low power but long irradiation, where the threshold is reached with lower temperature. Figure 2.13 explains this relation.
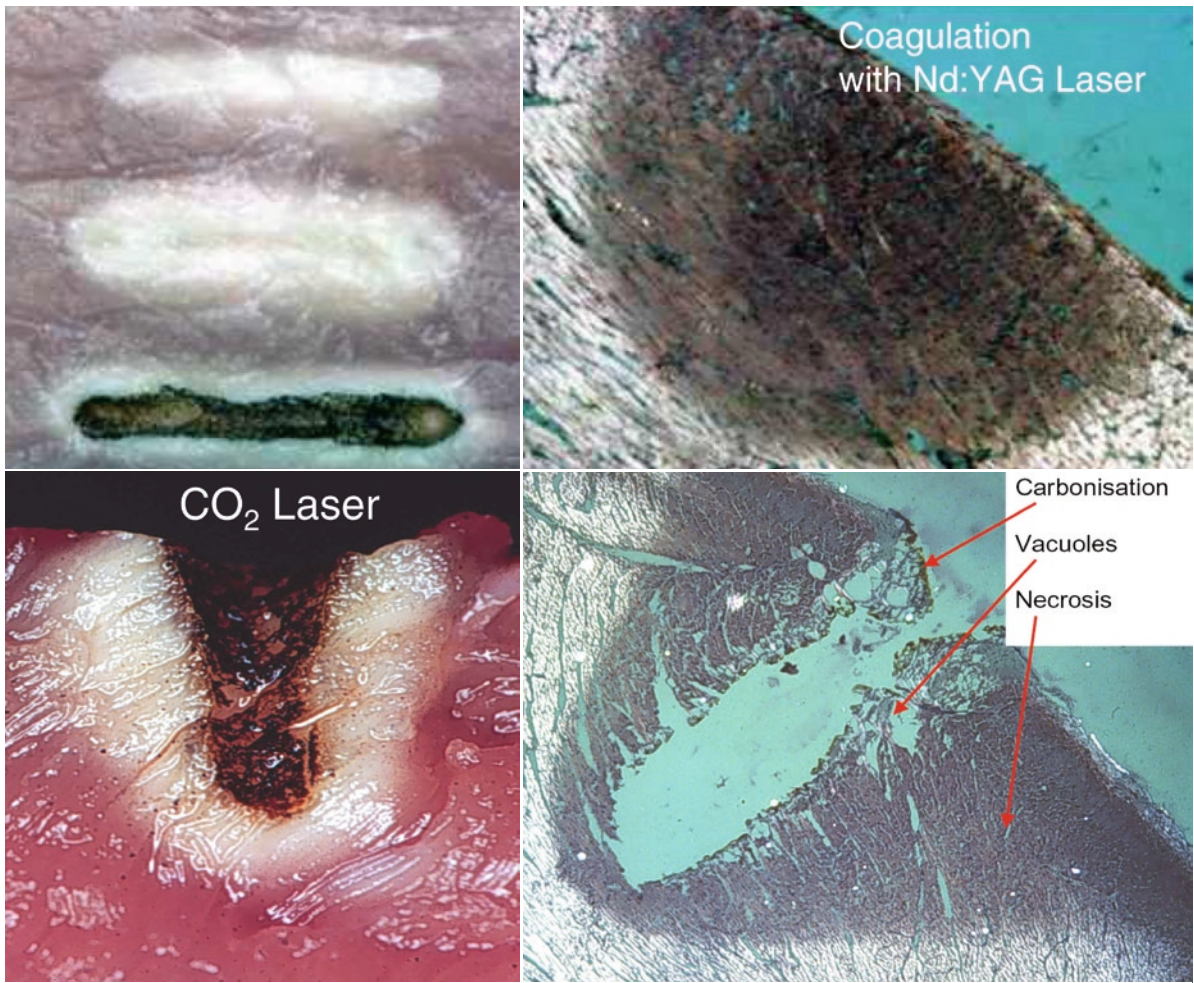
Fig. 2.12 Tissue effects of coagulation and vaporization with corresponding histologies. *CO₂* carbon dioxide, *Nd:YAG*, neodymium-doped yttrium aluminium garnet

Table 2.2 Thermal constants for different biological tissues and materials

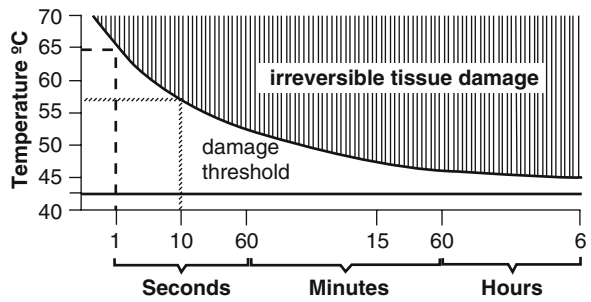| Material	Density ρ (g/cm³)	Water content (%)	c_w (J/g K)	Λ (W/m K)
Water	1,000	100	4.183	0.58
Blood	900	55	3.22	0.62
Fat	900	–	1.93	0.3
Cartilage	1,225	60–70	3.06	0.36
Liver	1,200	80	3.42	0.44
Aorta	1,000	80	3.76	0.48
Copper	8,933	–	0.383	384
Diamond	3,510	–	0.502	33,000

Fig. 2.13 Time-temperature characteristic of tissue damage. The threshold for tissue damage at different temperatures depends on laser power and application time. A 1-s pulse reaches the threshold at 65°C, whereas a 10-s pulse reaches the threshold at 57°C

Example:

The carbon dioxide laser is used in microsurgery for cutting tissue. We want to know the cutting depth by vaporization of the tissue with $p = 60$ W, focused to a spot size diameter of 0.4 mm and moved with a velocity of 2 cm/s [4]. Let E_c be the energy for heating the tissue to the boiling point and E_v the latent energy for vaporization per unit volume.

$$E_c = \rho c_w \Delta T \,[\text{J}],$$

where ρ is the density (here, 1,000 kg/m³ for water), c_w is the specific heat (4,200 J/kg°K), and ΔT is the difference between the boiling point and body temperature (~63°K).

$$E_v = \rho L_v,$$

where L_v is the latent heat for evaporation (2.3×10^6 J/ kg). The evaporated volume per unit time is then

$$V = P / \left(E_v + E_c \right) = d \cdot v \cdot d_{cut}.$$

Hence,

$$d_{cut} = P / dv \left(E_v + E_c \right).$$

With the parameters above for laser power, P, spot size, d and velocity, v, one calculates a cutting depth (d_{cut}) of 3 mm.

This value, of course, is overestimated because we neglected reflection, tissue components other than water, reabsorption by evaporating material, and energy dissipation. Nevertheless, it gives an estimation of the laser reaction on cutting tissue.

2.4.1 Relaxation Time

When the thermal diffusion length, L, is equal to the optical penetration depth, then we have the relation:

$$L = \left(4\kappa t \right)^{1/2},$$

where κ is the diffusivity with its value for water of 1.4×10^{-3} cm²/s. When $t = 1$ s, then $L = 0.8$ mm. Taking the optical tissue penetration $1/\mu_a$ as characteristic dimension, we get for the relaxation time:

$$\tau_R = 1/(4\mu_a \kappa).$$

For a carbon dioxide laser, wavelength 10.6 μm, with $\mu_a = 500$ cm⁻¹ and $\kappa = 10^{-3}$ cm²/s, one gets a relaxation time (τ_R) of 1 ms.

2.5 Tissue Ablation

The preconditions for tissue ablation are high absorption and very short laser pulses. Analogous to the *thermal confinement,* one can define a *stress confinement* when tissue is heated up so fast that the pulse duration is shorter than the propagation time, t_m, of the stress wave through the heated volume. The internal stress is described by the *Grüneisen coefficient*, Γ:

$$\Gamma = \alpha/(\rho c_w \kappa_T),$$

where α is the coefficient of thermal expansion, ρ is the density, c_w is the specific heat, and κ_T is the isothermal compressibility. The propagation time, t_m, of the stress wave through the heated tissue volume is

$$t_m = 1/\left(c_a \mu_a \right) [\text{s}],$$

where c_a is the speed of sound in the medium. When the stress wave with velocity c_a cannot leave the heated volume during the laser pulse, then it is removed with the ablation of the material and the surrounding tissue is not damaged.

For the photoablation process, a simple model has been derived to calculate the ablation depth [8, 17]. It is called the "blow-off" model. To ablate tissue, an ablation threshold must be surmounted. The ablation depth, d, per laser pulse is determined by the pulse energy until a saturation threshold. The assumption is that there exists a threshold $F_s(d)$ for the energy density. Below this threshold, no material is removed.

Ablation threshold: $F_s(d) = F_0 \exp(-\mu_a d)$.
The solution for the ablation depth, d, can simply be derived from this expression:

$$d = \left(1/\mu_a \right) \ln \left(F_0 / F_s \right).$$

Figure 2.14 explains graphically the threshold behaviour, and Fig. 2.15 gives a demonstration of the ablation process with supersonic particle ejection and the ablated crater in dental hard tissue. Only UV lasers (ArF excimer laser) and pulsed MIR lasers have such high tissue absorption that they are effective ablating lasers.
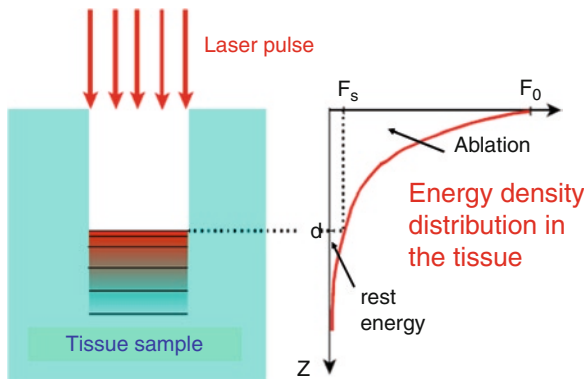
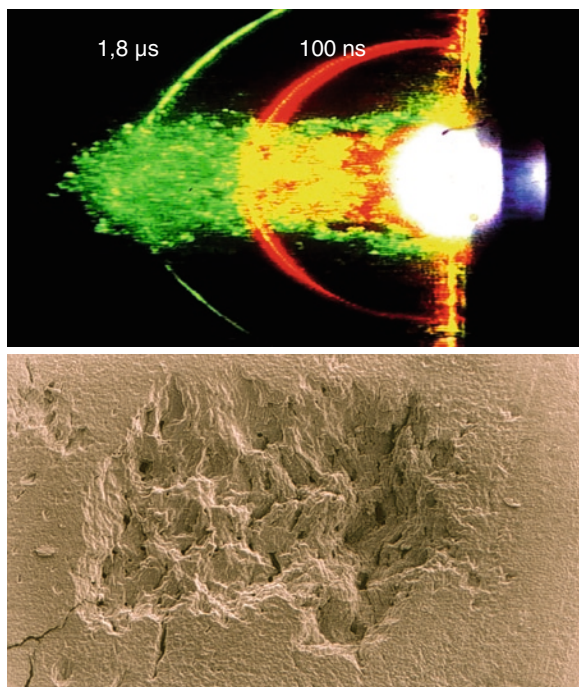Fig. 2.14 Schematic representation of the blow-off model

Fig. 2.15 Picture of the ablation process (*top*) and the crater in hard dental material (*bottom*)

The threshold behaviour of highly absorbed laser radiation, e.g., the erbium-doped yttrium aluminium garnet (Er:YAG) laser with a 2,940-nm wavelength, can be used to modulate the thickness of necrosis in soft tissue. Operation of the laser in normal ablation mode does not produce effective thermal necrosis; therefore, no coagulation can stop bleeding. The advantage is that the healing is fast with minimal scarring. However, for precise superficial surgical interventions, it would be helpful if the Er:YAG laser also could coagulate the tissue

and stop bleeding. This is possible by applying between the ablating laser pulses a series of high-frequency sub-threshold laser pulses. The energy of such pulses is below the ablation threshold and therefore is transferred into heat. The heat causes thermal necrosis. The thickness of the necrotic tissue layer can be modulated by the number of sub-threshold pulses. Some Er:YAG laser systems have such operation modes, which are well accepted for microsurgery procedures.

In Fig. 2.16, the addition of the laser pulse heating effect is demonstrated. Certain levels of temperature can be attained, producing thermal necrosis.

A good summary and overview of laser-tissue interaction is the graph in Fig. 2.17. Here, the duration of laser application of duration of laser pulses is plotted for different laser types and their corresponding depth of penetration of biological tissue. Areas are marked for normal thermal reactions, thermal confinement – the pulse duration is shorter than the thermal diffusion length or thermal relaxation time – and stress confinement for ultrashort laser pulses.

2.6 Photodisruption

Focused laser pulses in the nanosecond region (e.g., with a Q-switch neodymium (Nd):YAG laser), or with picosecond or femtosecond durations (titanium (Ti) sapphire laser) develop power densities of 10^{12} W/cm² and more. The electric field strength of this focused radiation is high enough to pull electrons out of the atoms, forming a plasma and producing an optical breakdown with shockwaves disrupting the tissue. The process of this photomechanical reaction is described in detail by Boulnois [3] and Vogel and Venugopalan [17].

Above a light intensity of 10^{11} W/cm², an increased and nonlinear absorption of the light occurs, accompanied by an intense white flash and an acoustic signal – an optical breakdown happens with plasma formation. Multiphoton absorption is responsible for the ionization of atoms. The effect is intensity dependent and scales with I^4. The free electrons are accelerated in the intense electromagnetic field (inverse Bremsstrahlung), and secondary electrons are produced through collision ionization (Avalange effect; see Fig. 2.18). The heated electrons and ions form the plasma of 15,000–20,000° K and a pressure of 20–60 bar. It follows

Fig. 2.16 Temperature
profiles created by sub-
threshold erbium-doped
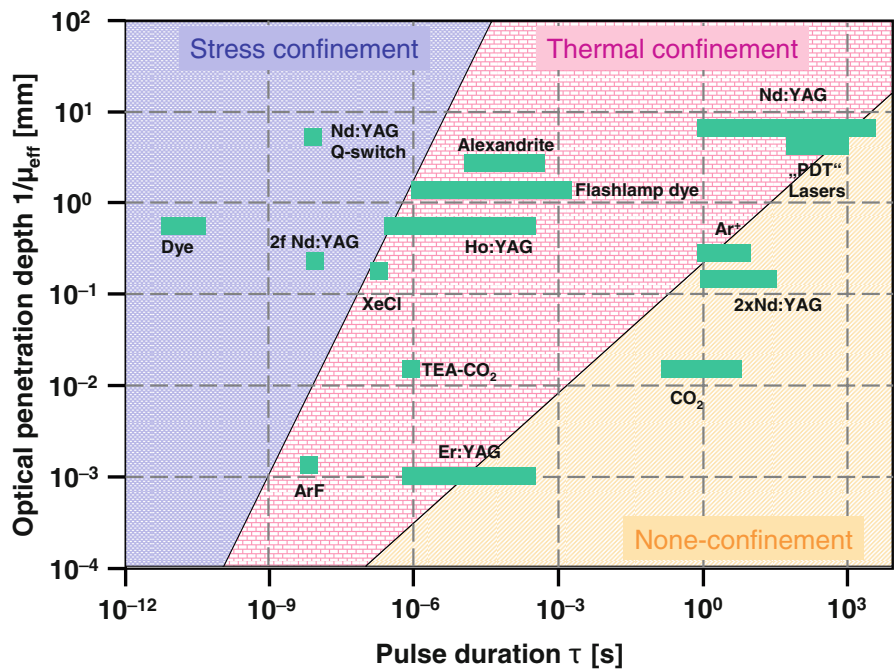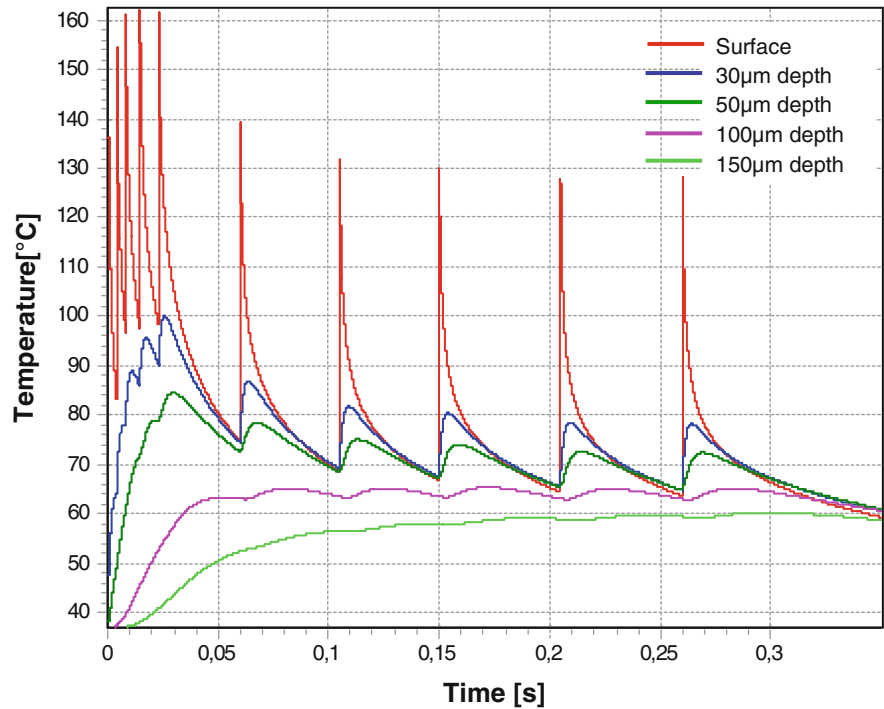yttrium aluminium garnet
laser pulses

Fig. 2.17 Schematic of laser
types, the corresponding tissue
reactions, pulse duration, and
optical penetration depth

a cavitation bubble of water vapour; the dimension of it depends on the pulse energy and pulse duration. The shorter the pulse, the smaller may be the energy to get an optical breakdown. Hence, the cavitation bubble also will be smaller, and the side effects will be reduced.

The length of the plasma, Z_{max}, created by a focused Gaussian beam, is determined by the Rayleigh length of the focus, Z_R, and the relation of the pulse intensity to the threshold intensity, I_0/I_{th}, for an optical breakdown.

Plasma length: $Z_{max} = Z_R \cdot (I_0/I_{th} - 1)^{1/2}$

10^{12} W/cm^2 in focus area
Free electron generation: $N_e > 10^{12}$ cm^{-3}
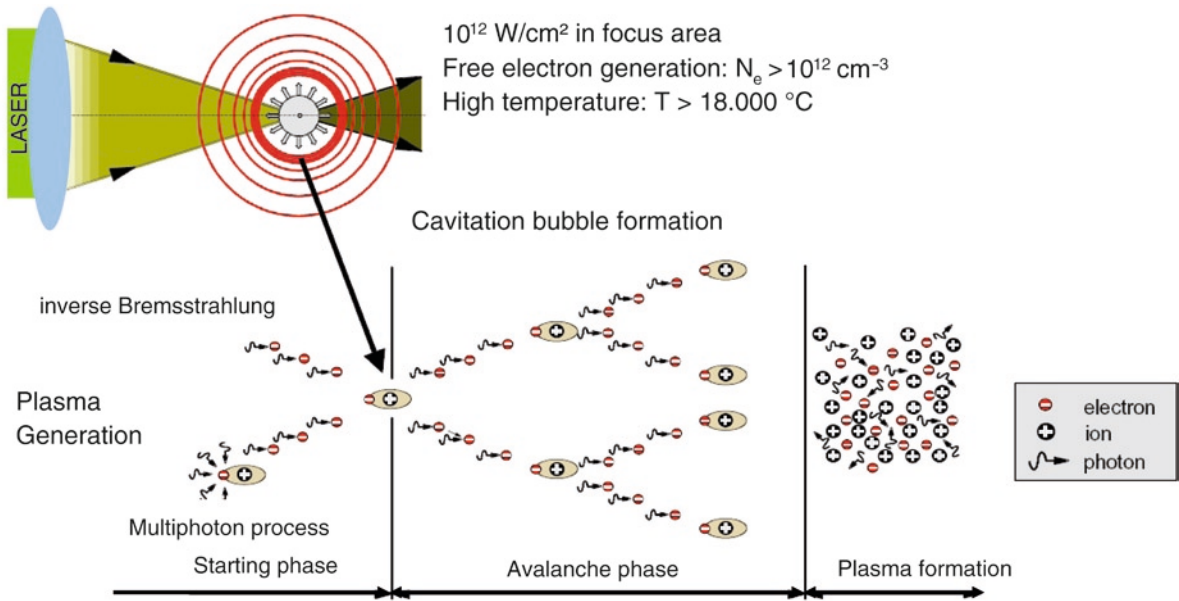High temperature: T > 18.000 °C

Fig. 2.18 Schematic presentation of the processes responsible for the optical breakdown generated by ultrashort laser pulses
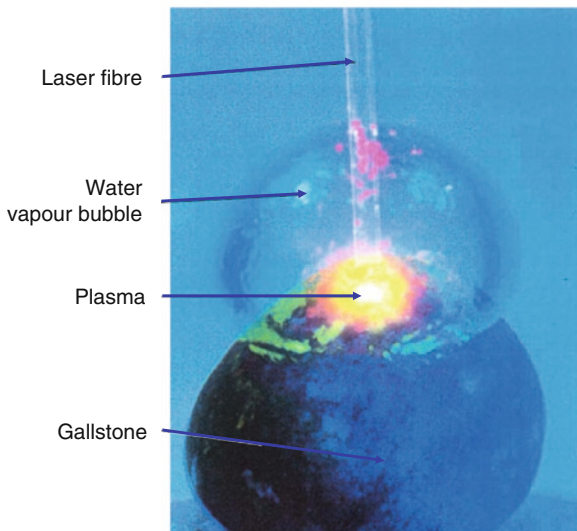

Fig. 2.19 Picture of an optical breakdown with plasma and cavitation bubble [9]

where Z_R is the Rayleigh length, $Z_R = \pi\omega_0^2/\lambda$, with beam waist ω_0 and λ the wavelength in the medium, corrected with the refractive index.

The example of a high-speed camera picture is taken from Ihler [9]. It shows the reaction of a pico-second laser pulse on a gallstone. The laser pulse is guided through a fibre to the stone. The plasma formation and the cavitation bubble are clearly visible.

The bubble has its maximum dimension after about 300 μs, then it collapses, and normally a multiple rebound effect occurs (Fig. 2.19).

Medical applications of ultrashort laser pulses (100 fs, Ti:sapphire laser) are found in ophthalmology for cutting flaps of the cornea. Soft and hard tissue removal can be done very precisely, but the efficiency is not very high. Therefore, most applications of multiphoton absorption are in microscopy and tissue diagnostics.

Take Home Pearls

› Be sure to use a laser with the right wavelength, power or energy, and pulse regime for your specific application.
› Consider depth of penetration of the light into the tissue and the quadratic power density dependence with the distance (spot size).
› Take the zone of necrosis for blood coagulation into consideration.
› Less laser power is sometimes better to prevent uncontrollable side effects.
› With only one laser device you are limited in your dermatologic applications; do not try to extend it for other applications because you will fail.

References

1. Anderson RR, Parish JA. Selective photothermolysis: precise microsurgery by selective absorption of pulsed radiation. Science. 1983;220:524–7.

2. Anderson RR, Margolis RJ, Watanabe S, Flotte T, Hruza GJ, Dover JS. Selective photothermolysis of cutaneous pifmentation by Q-switched Nd:YAG laser pulses at 1064, 532 and 355 nm. J Invest Dermatol. 1989;93:28–32.

3. Boulnois JL. Photophysical processes in recent medical laser developments: a review. Lasers Med Sci. 1986;1:47–66.

4. Cammarata F, Wautelety M. Medical lasers and laser-tissue interactions. Phys Educ. 1999;34:156–61.

5. Gao X, Xing D. Molecular mechanisms of cell proliferation induced by low power laser irradiation. J Biomed Sci. 2009;16:4.

6. Hawkins-Evans D, Abrahamse H. A review of laboratory-based methods to investigate second messengers in low-level laser therapy (LLLT). Med Laser Appl. 2009;24: 201–15.

7. Henyey LG, Greenstein JL. Diffuse radiation in the galaxy. Astrophys J. 1941;93:70–83.

8. Hibst R. Technik, Wirkungsweise und medizinische Anwendungen von Holmium- und Erbium-Lasers. In: Fortschritte der Medizin 15, Müller, Berlin eds, ecomed verlagsgesellschaft AG & Co.KG, Landsberg; 1997.

9. Ihler B. Laser Lithotripsie-Untersuchung der in-vitro Fragmentierung mit Mikrosekunden-Impulsen, Dissertation Universität Karlsruhe; 1992.

10. Jacques S. The role of tissue optics and pulse duration during high-power laser irradiation. Appl Opt. 1993;32:2447–54.

11. Karu TI. Low-power laser therapy. In: Vo-Dinh T, editor. Biomedical photonics handbook. London: CRC Press; 2003. p. 48–250.

12. Romero LF, Trelles O, Trelles MA. Real-time simulation for laser-tissue interaction model, NIC Series 2006;33: 415–422.

13. Steiner R. Thermal and non-thermal laser-dissection. End Surg. 1994;2:214–20.

14. Steiner R. Interactions of laser radiation with biological tissue. In: Berlin HP, Müller GJ, editors. Applied laser medicine. Berlin: Springer; 2003. p. 101–6.

15. Steiner R, Melnik IS, Kienle A. Light penetration in human skin: in-vivo measurements using isotropic detectors. SPIE. 1993;1881:222–30.

16. Thomsen S. Pathologic analysis of photothermal and photomechanical effects of laser-tissue interactions. Photochem Photobiol. 1991;53:825–35.

17. Vogel A, Venugopalan V. Mechanisms of pulsed laser ablation of biological tissues. Chem Rev. 2003;103:577–644.

18. Wang L, Jacques SL, Zheng L. MCML – Monte Carlo modeling of light transport in multi-layered tissues. Comput Methods Programs Biomed. 1995;47:131–46.